NASA Technical Paper 2894

1989

Contamination of Liquid Oxygen by Pressurized Gaseous Nitrogen

Allan J. Zuckerwar
Langley Research Center
Hampton, Virginia

Tracy K. King
and Kim Chi Ngo
Old Dominion University
Norfolk, Virginia

NASA
National Aeronautics and Space Administration
Office of Management
Scientific and Technical Information Division

Introduction

The modified Langley 8-Foot High-Temperature Tunnel (8' HTT) will utilize pressurized gaseous nitrogen (GN_2) at about 2000 psig to transfer liquid oxygen (LOX) from a run tank to the tunnel combustor. Since the contamination of the LOX by pressurized GN_2 may prove to be an important operational constraint, it is desirable to have reliable data concerning the penetration of nitrogen into LOX during pressurization. Such data, unfortunately, are scanty or nonexistent.

Contamination of the LOX takes place through the following process. When GN_2 is first admitted to the run tank, it cools down rapidly to near the LOX temperature ($\approx$ 90.2 K). When the pressure reaches approximately 52 psia, a layer of liquid nitrogen (LN_2) builds up at the LOX interface. The LN_2 penetrates into the LOX primarily by simple molecular diffusion. The purpose of this study is to determine experimentally the extent of the penetration of LN_2 into LOX under given operating conditions.

The principle of the measurement is based on a technique known as "differential flash vaporization" (ref. 1), whereby a two-component liquid is permitted to evaporate and the vapor formed is removed from the remaining liquid. An analysis of the vapor yields sufficient information to determine the initial composition of the liquid, from which the binary diffusivity can be obtained. The adaptation of this technique to the present experiment, which was conducted in one of the 4-gal run tanks of the Langley 7-Inch High-Temperature Tunnel (the pilot tunnel for the 8' HTT), is illustrated in figure 1. After the run tank is filled with LOX to a specified level, the test consists of three basic steps:

1. Pressurization—the run tank is pressurized with GN_2 for a specified holding time
2. Blowdown—the pressurized GN_2 is vented to 0 psig
3. Analysis—the vapor from the evaporating liquid is analyzed in an oxygen analyzer, and a time history of the O_2 content is recorded for subsequent data processing.

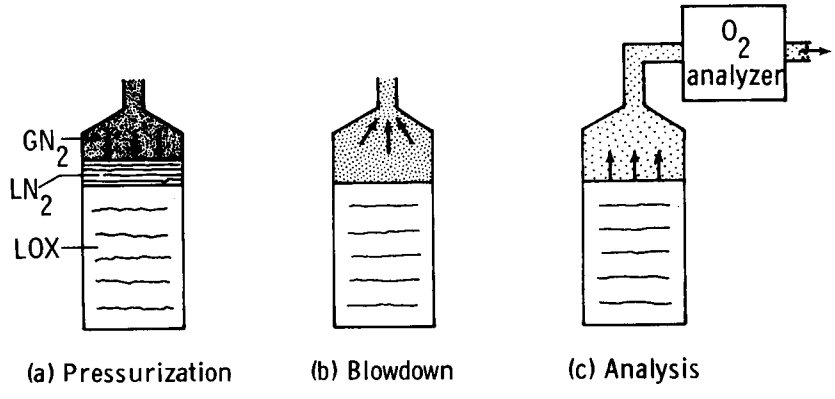

Figure 1. Principle of the differential flash vaporization technique.

This paper is organized into three basic parts: theory, experiment, and results. The theory includes a physical model of the LOX contamination process and a derivation of the equations used to evaluate the diffusivity from the data. The experimental sections contain first an account of a preliminary experiment, using a nuclear monitor, to study the buildup of the LN_2 layer under pressurization, and then a description of the experimental procedure used in the differential flash vaporization experiment. The results include the evaluation of the diffusivity, error analysis, application to operating conditions in the 8' HTT, and comparison with prior measurements at lower temperatures.

The authors express their thanks to Andrew P. Seamons, Governor's School for the Gifted, 1987, for assistance in making the measurements.

Symbols

A	surface area of liquid, cm^2
b_1, b_2, b_3	parameters to fit pressure time history
D	binary diffusivity of LOX-LN_2 mixtures, cm^2/sec

D_0	preexponential factor, cm^2/sec
h	diffusion length (penetration depth), cm
n_L	total number of moles of liquid, mol
n_V	total number of moles of vapor in ullage volume, mol
P	total pressure in the run tank, psig
P_o	reference pressure for flow rate calibration, atm
P_1	pressure at the flowmeter, atm
R	evaporation rate, mol/min
R_g	universal gas constant, cm^3-atm/mol-K
R_o	reference flow rate, cm^3/min
T	temperature of vapor in ullage volume, K
T_L	temperature of the liquid, K
T_o	reference temperature for flow rate calibration, K
T_1	temperature at the flowmeter, K
t	time, min
t_h	holding time, min
t_M	time at inflection point, min
V	ullage volume, cm^3
v_L	molar volume of liquid, cm^3/mol
v_{LN}	molar volume of LN_2, cm^3/mol
v_{LX}	molar volume of LOX, cm^3/mol
x_N	mole fraction of N_2 in the vapor
x_{NL}	mole fraction of N_2 in the liquid
x_{N0}	value of x_{NL} at time $t = 0$
Z	location along the run tank, in.
z	distance from interface, cm
z_i	interface location at any time, cm
z_0	interface location at time $t = 0$, cm
ΔH	activation enthalpy, kcal/mol
κ	coefficient of volume expansion, K^{-1}
ρ_L	liquid density, g/cm^3
τ_1	time constant to flush out ullage volume, min
τ_2	characteristic evaporation time, min
τ_R	value of τ_1 at unit pressure, min
Subscript:	
M	indicates inflection point

Superscript:

$'$	(prime) indicates quantity for holding time of 1 min

Mathematical functions:

$\mathrm{erf}(x)$	error function, $(2/\sqrt{\pi}) \int_0^x e^{-u^2}\, du$
$\mathrm{erfc}(x)$	complementary error function, 1 – $\mathrm{erf}(x)$
$\mathrm{erf}^{-1}(x)$	inverse error function

Note on units: Quantities read directly from tunnel instrumentation retain the units of the instrumentation, usually English units. Quantities used in the evaluation of the data are expressed in metric units.

Theoretical Background

Physical Model of the LOX Contamination and Monitoring Processes

The model is described with the aid of figure 2, showing the N_2 profile during pressurization, blowdown, and analysis. Prior to pressurization the run tank is filled with LOX to a specified level. After pressurization a layer of LN_2 builds up at the LOX interface. The concentration profile of LN_2 immediately after pressurization is indicated by curve A in figure 2(a). The origin $z = 0$ is chosen as the LOX-LN_2 interface location. Initially the run tank contains pure LOX for $z > 0$ (toward the bottom) and pure LN_2 for $z < 0$ (toward the top).

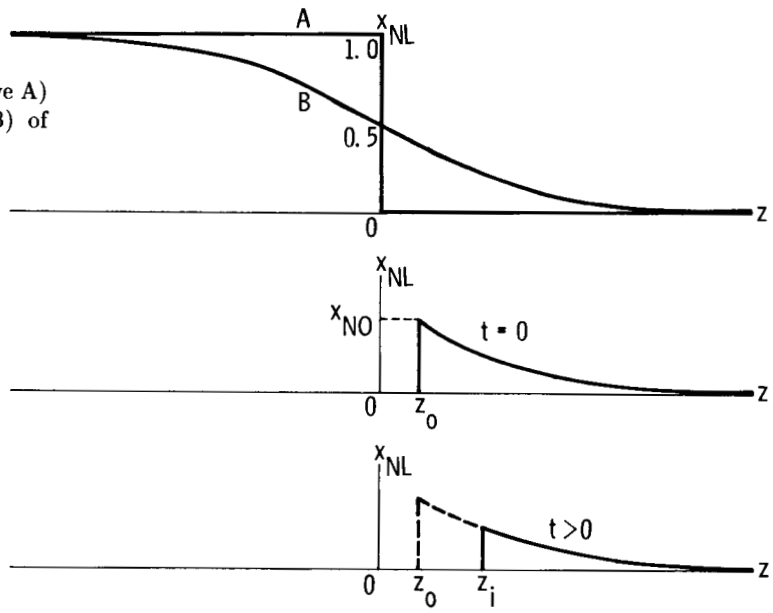

(a) At the beginning (curve A) and completion (curve B) of pressurization.

(b) Just after blowdown.

(c) During analysis.

Figure 2. Distribution of LN_2 in the run tank during the three steps of the experiment.

The large concentration gradient across the interface results in mass transport by molecular diffusion. After a given holding time the LN_2 concentration profile is given by curve B, indicating that the LN_2 has penetrated into the region formerly occupied by the pure LOX. The quantity of LN_2 passing into this region increases with increasing holding time. Curve B, representing a typical LN_2 concentration profile at the end of the pressurization step, is described mathematically as a complementary error function (ref. 1):

$$x_{NL} = \left(\frac{1}{2}\right) \mathrm{erfc}\left(\frac{z}{2\sqrt{D\,t_h}}\right) = \left(\frac{1}{2}\right)\left[1 - \mathrm{erf}\left(\frac{z}{2\sqrt{D\,t_h}}\right)\right] \tag{1}$$

where D is the diffusivity and t_h the holding time.

During blowdown the falling pressure quickly reaches a level that can no longer sustain N_2 in the liquid state, and the N_2-rich portion of the liquid immediately evaporates. When the pressure finally reaches 0 psig,

the liquid has evaporated to some point z_0 below the original interface location as the result of N_2 penetration into the LOX. The concentration profile immediately at the end of blowdown is illustrated in figure 2(b). At this time (defined as $t = 0$) vapor from the evaporating liquid is routed to the oxygen analyzer.

During the analysis step the interface location z_i shifts steadily from its initial location z_0 toward the bottom of the run tank (increasing z). At any time $t > 0$ the composition of the vapor is representative of that of the interface location from which it has evaporated. The steadily progressing shift in interface location is illustrated in figure 2(c).

Simplifying Assumptions

A mathematical description of the events depicted in figures 1 and 2 is intractably complex but can be made feasible with the aid of several simplifying assumptions:

1. During pressurization there is no thermal (Soret effect) or convective mixing of the liquids. The temperature difference between the LOX and the LN_2 at the interface is too small to provide a significant driving force for thermal diffusion. Convective mixing ensues from an instability developing between two opposing effects. The natural buoyancy due to the lower density of LN_2 compared with LOX, 0.7912 vs. 1.167 g/cm^3 (under pressurization), is a stabilizing effect. The lateral temperature gradient, due to the temperature difference between the wall of the run tank (77.4 K) and the core of the liquid (90.2 K), is destabilizing in that it causes thermal buoyancy which tends to initiate a circulating axial flow. If one adopts the criterion that the thermal buoyancy must exceed the natural buoyancy for convective mass transfer to occur, then the thermal Grashof number must exceed the concentrative Grashof number (see ref. 1, p. 66). The ratio of these numbers is $\rho_L \kappa \Delta T_L / \Delta \rho_L$, which in the present case has the value, in cgs units,

$$\frac{1.167 \times 0.0038 \times 12.8}{1.167 - 0.7912} = 0.15 < 1$$

   indicating a high degree of stability against convective mass transfer.
2. There is no net molecular transport across the interface; that is, for every N_2 molecule that crosses from above, a corresponding O_2 molecule crosses from below. The practical significance of this assumption is that the interface location shown in figure 2(a) does not change during pressurization. This manner of transport is known as "equimolar counter diffusion," which is characterized by a single coefficient known as the "binary diffusivity."
3. The concentration profile of the liquid remains frozen after blowdown. The LN_2 remaining after blowdown in figures 2(b) and 2(c) follows the profile at the end of the pressurization interval, curve B in figure 2(a). The justification for this assumption is that the concentration gradient is too small, except at the rapidly evaporating leading edge, to permit significant diffusion after blowdown.
4. Evaporation of the liquid proceeds at a constant rate R. Actually, as will be shown later, this condition can be enforced since the evaporation rate can be adjusted by means of a hand valve. Consequently, the interface location z_i advances linearly with time:

$$z_i = z_0 + R v_L t / A \tag{2}$$

   where R is the evaporation rate, v_L the molar volume, and A the cross-sectional area of the liquid.
5. The steady-state vapor flow rate is constant and equal to the evaporation rate. In other words, after blowdown, pressure does not build up in the run tank. As will be seen, this assumption is not quite valid, but a method for correcting for a slow pressure buildup is described in appendix B. In any case, a breakdown of this assumption has minimal impact upon the evaluation of the diffusivity.
6. The vapor in the ullage volume, i.e., the volume of the run tank above the liquid plus that of the system piping, is homogeneous. Vapor from the evaporating liquid mixes very rapidly with that already present in the ullage volume. The O_2 analyzer samples the homogeneous vapor mixture.
7. The ullage volume is constant. Because most of the diffused N_2 is contained in a small volume near the interface, the essential information concerning LN_2 concentration is gathered from the initial small fraction of the evaporating liquid after blowdown.

Analysis

In figure 1(c) let n_V be the total number of moles of vapor in the ullage volume and n_L the total number of moles of liquid. Conservation of molar content requires, as the liquid evaporates, that

$$\frac{dn_V}{dt} = -\frac{dn_L}{dt} = R \tag{3}$$

Similarly, conservation of moles of N_2 requires that

$$\frac{d}{dt}(x_N n_V) = -\frac{d}{dt}(x_{NL} n_L)$$

$$x_N \frac{dn_V}{dt} + n_V \frac{dx_N}{dt} = -x_{NL} \frac{dn_L}{dt} - n_L \frac{dx_{NL}}{dt} \tag{4}$$

where x_N and x_{NL} are the mole fractions of N_2 in the vapor and liquid, respectively. At this point the analysis takes a different course from that taken in conventional flash vaporization. In the latter the liquid is a homogeneous mixture of two components. As the liquid evaporates, the mole fraction of the more volatile component in the vapor changes very slowly. Thus dx_N/dt is assumed small, and the second term in equation (4) is neglected.

In the present experiment the situation is considerably different. The liquid is not a homogeneous mixture; rather, x_{NL} is strongly spatially dependent and x_N changes rapidly with time. As a consequence of assumption (3) (frozen LN_2 profile), on the other hand, x_{NL} does not change with time:

$$\frac{dx_{NL}}{dt} = 0 \tag{5}$$

and the last term in equation (4) vanishes. Substitution of equations (1), (3), and (5) into (4) leads to the following transport equation at the interface $z = z_i$:

$$n_V \frac{dx_N}{dt} + R x_N = R x_{NL} = \frac{R}{2}\left[1 - \text{erf}\left(\frac{z_i}{2\sqrt{D\,t_h}}\right)\right] \tag{6}$$

Upon defining, for convenience,

$$h = 2\sqrt{D\,t_h} \tag{7}$$

$$\tau_1 = \frac{n_V}{R} \tag{8}$$

$$\tau_2 = \frac{A\,h}{R\,v_L} \tag{9}$$

and using equation (2), one can rewrite equation (6) in more simplified form:

$$\frac{dx_N}{dt} + \frac{x_N}{\tau_1} = \frac{x_{NL}}{\tau_1} = \frac{1}{2\tau_1}\left[1 - \text{erf}\left(\frac{z_0}{h} + \frac{t}{\tau_2}\right)\right] \tag{10}$$

Each of the convenience variables defined in equations (7)–(9) has a physical meaning: h is the diffusion length, or "penetration depth" corresponding to the holding time t_h; τ_1 is the time constant for flushing the GN_2 out of the ullage volume; and τ_2 is a characteristic "evaporation time" representing the rate of advance of the interface. Noteworthy is the fact that, among the characteristic times, only τ_2 contains h and thus information regarding the diffusion constant.

The initial condition is expressed in terms of the mole fraction of N_2 in the liquid at the end of blowdown, in other words, at the time the analysis begins. Using equations (1) and (2), one expresses this condition as

$$x_{N0} = x_{NL}(0) = \frac{1}{2}\left[1 - \text{erf}\left(\frac{z_0}{h}\right)\right] \tag{11}$$

This is indicated in figure 2(b). Details of the solution to equation (10), together with initial condition (11), are given in appendix A. The solution is

$$x_N(t) = \frac{1}{2}\left[1 - \operatorname{erf}\left(\frac{z_0}{h} + \frac{t}{\tau_2}\right)\right] + \frac{1}{2}\exp\left[-\left(\frac{t}{\tau_1} + \frac{z_0\tau_2}{h\tau_1} - \frac{\tau_2^2}{4\tau_1^2}\right)\right] \times \left[\operatorname{erf}\left(\frac{t}{\tau_2} + \frac{z_0}{h} - \frac{\tau_2}{2\tau_1}\right) - \operatorname{erf}\left(\frac{z_0}{h} - \frac{\tau_2}{2\tau_1}\right)\right] \quad (12)$$

In sum, equation (12) represents the time dependence of the mole fraction of N_2 in the ullage volume—in other words, the mole fraction that is detected in the oxygen analyzer.

Preliminary Investigation of the LOX-LN_2 Interface Profile

A test to gather information concerning the structure of the LOX-LN_2 interface profile was conducted using a nuclear monitor developed by Singh, Davis, and Mall (ref. 2). This monitor is capable of identifying the medium—LOX, LN_2, or vapor—at any location within the run tank.

The test setup is illustrated in figure 3. A Cs^{137} source emits a collimated beam of 662 keV γ-radiation to a NaI detector on the opposite side of the run tank. The detector counts the number of emissions within a given time interval. The beam is attenuated by the steel wall of the run tank as well as by the medium within the wall. Despite a rather high attenuation in the former, the detection system is still sensitive enough to distinguish among attenuation differences in LOX, LN_2, and vapor. Table I shows the number of 15-sec counts with each of these three media contained in the space within the wall, together with their standard deviations. It is clear that the count yields an unambiguous identification of the medium. The source and detector are mounted on a rigid frame, which slides along a track. The frame can be locked at any location Z, as measured by a scale along the tank from 0 to 100 in. The tank extends an additional 28 in. beyond either end, regions which are not accessible to the monitor.

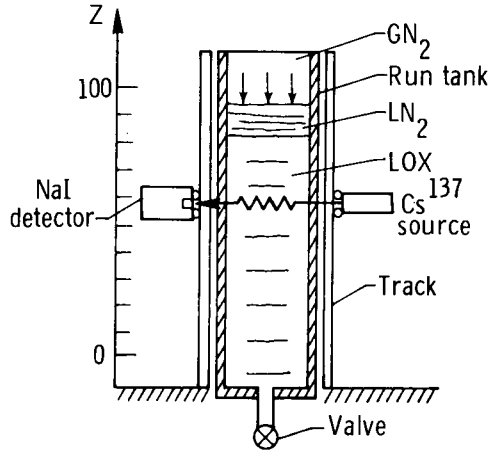

Figure 3. Test setup for the preliminary investigation of the LOX-LN_2 interface profile. The 45° slant of the run tank is not shown.

Table I. Number of 15-sec Counts of Cs^{137} (662 keV) Gamma Rays Passing Through Various Media

Medium	Number of counts
LOX	6700 ± 161
LN_2	8300 ± 161
Vapor	10 500 ± 95

In the interface profile tests the nuclear monitor was fixed at a location $Z = 50$ in., halfway along the run tank. The run tank was precooled with LN_2, emptied, and filled with LOX to the 50-in. level, as determined by a change in count on the monitor. After GN_2 was admitted to the run tank to a predetermined pressure, the

monitor was moved to identify the medium at selected locations starting at $Z = 30$ in. A typical result is shown in figure 4 for a GN_2 pressure of $P = 750$ psig. At each location a set of three 15-sec counts was recorded, and the monitor was then moved to the next location. After the measurements at $Z = 100$ in. (top of the track), the monitor was moved back to $Z = 55$ in. to confirm the previous readings. The count indicates the presence of LOX between 30 and 50 in., a transition region from 50 to 55 in., and a layer of LN_2 between 55 and 70 in. At locations of 85 and 100 in. the count is too high for LN_2 but too low for vapor. The interpretation of these values is based on the fact that the run tank becomes warmer near the top. At locations above 70 in. the temperature apparently exceeds the critical temperature, and N_2 exists in the supercritical state with decreasing density toward the top of the run tank.

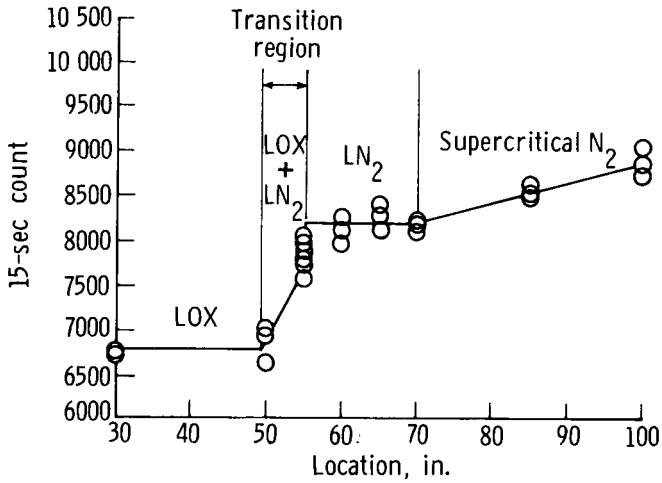

Figure 4. Interface profile at a GN_2 pressure of $P = 750$ psig.

The test was repeated for GN_2 pressures of 250, 500, 1200, and 1800 psig. The corresponding layers of LN_2 above the interface measured 3, 10, 30, and 40 in., respectively. For the present discussion, N_2 at temperatures near 90 K is considered a liquid even at pressures beyond the critical pressure of 492 psia. In conclusion, under pressurization a layer of LN_2 builds up at the LOX interface to a level where the temperature is too high to support the liquid. Since density at the interface conforms to that of the liquid rather than the vapor, a consequence of the LN_2 buildup at the interface is enhanced mass transport through molecular diffusion.

Experimental Procedure

The LOX-LN_2 contamination experiments were carried out at the Langley 7-Inch High-Temperature Tunnel, the pilot tunnel for the Langley 8-Foot High-Temperature Tunnel. The experimental setup is shown in figure 5. The piping in the system, with the exception of coils 1 and 2, was oxygen-cleaned and inspected. The tests consisted of four major steps: (1) setup, (2) precooling of the run tank, (3) pressurization and blowdown, and (4) monitoring.

During the setup step of each test the monitoring instrument, a Beckman Model 755 oxygen analyzer (0–100%), was calibrated, and the nuclear monitor was installed. Calibration procedures required the use of the 3-way valve D shown in figure 5. Pure bottled GN_2 (99.995%) was used to calibrate the zero point, and bottled air was used to set the 20.9% O_2 point. The Beckman analyzer was checked on one occasion against uncontaminated evaporating LOX in the 4-gal run tank and yielded a reading of 99.992%. The nuclear monitor was installed at the 46-in. mark on the scale outside the run tank to give a liquid level indication for oxygen filling.

Since the thermal insulation of the run tank is not of Dewar quality, two methods were implemented to slow the evaporation of the LOX-LN_2 mixture. First the run tank was precooled by filling it completely with LN_2. After an ample cooling period, the LN_2 was discharged to the atmosphere. Second, LN_2 was injected through two copper tubes that coiled around the outside of the run tank as seen in the figure. The addition of the cooling coils decreased the evaporation rate by a factor of 5 compared with earlier experiments. At the end of the precooling period LOX was transferred immediately into the run tank and filled to the 46-in. level as measured by the nuclear monitor. Normally filling continued for 1 additional minute after this point was reached to ensure that the liquid level stabilized.

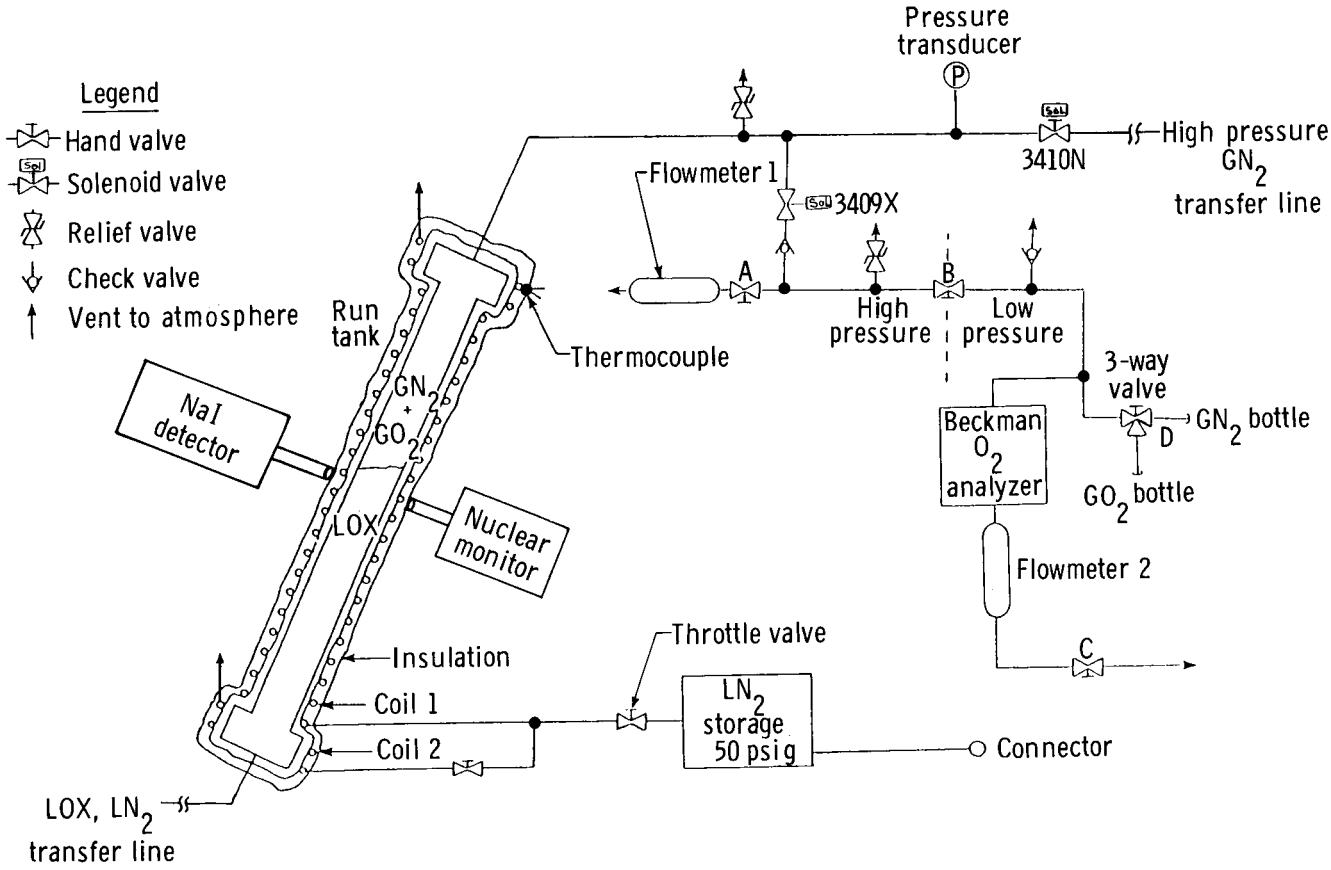

Figure 5. Test setup for the differential flash vaporization experiments.

The next step, pressurization and blowdown, began with pressurizing the top of the run tank with GN_2. Various GN_2 pressures and holding times, listed in table II, were used to study how these parameters affected the N_2 penetration into the LOX. After the GN_2 was held for the predetermined time, the pressure was vented to prepare for monitoring of the evaporating LOX-LN_2 through the Beckman analyzer.

Table II. Summary of Experimental Parameters

Run	N_2 pressure, psig	Holding time t_h, min	Comment
1	1700	15	Supercritical for both O_2 and N_2
2	1700	15	Supercritical for both O_2 and N_2
3	1700	15	Supercritical for both O_2 and N_2
4	1700	15	Supercritical for both O_2 and N_2
5	1700	15	Supercritical for both O_2 and N_2
6	1000	15	Supercritical for both O_2 and N_2
7	500	15	Supercritical for N_2 but not for O_2
8	1700	1	Supercritical for both O_2 and N_2
9	30	15	Normal

For the monitoring step the pressure in the run tank was vented to 0 psig before venting through the Beckman analyzer to ensure that the residual GN_2 was flushed out of the monitor line. After valve 3409X was opened the flow from the run tank proceeded through two parallel paths. The first path passed the bulk of the vapor through flowmeter 1 at 30 000 cm^3/min, as controlled by valve A, and was then vented to the atmosphere. The second path passed a sample through the Beckman analyzer and flowmeter 2 at 250 cm^3/min, as controlled by valve B, and then was also vented to the atmosphere. The flowmeter readings were continuously adjusted to

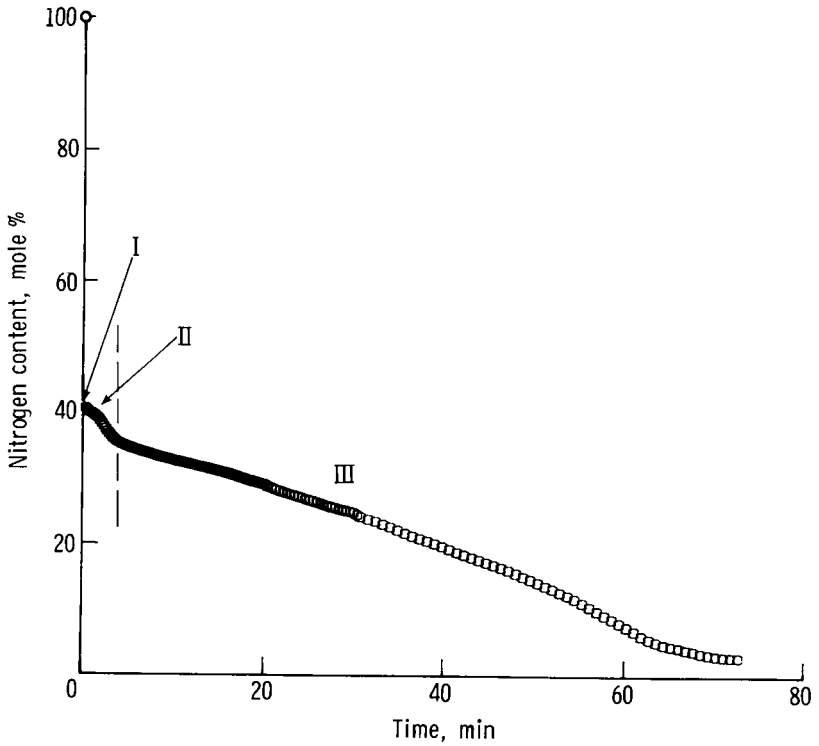

Figure 6. Time history of N_2 content in the vapor monitored by the Beckman O_2 analyzer for a typical run (Run 2). The GN_2 pressure was $P = 1700$ psig for a holding time of $t_h = 15$ min. Three regions are identified: I (0–1 min), adjustment time of the Beckman monitor; II (1–4 min), evaporation of the N_2-rich liquid; and III (> 4 min), flushing out of GN_2 from the ullage volume.

these fixed levels on each test run. Valve C was left open during each run and served only to prevent backflow from the atmosphere when the system was not in use.

For the remainder of the run, data were recorded that included the temperature of the cooling coils as measured by a thermocouple, the percent O_2 as measured on the Beckman analyzer, the pressure in the ullage volume, and the elapsed time. With the exception of the pressure, which was recorded manually, these measurements were recorded in 10-sec intervals by means of an Omega analog-to-digital converter interfaced to an Apple IIe computer system. The experiments ran until the Beckman analyzer reading neared 100% O_2 for a period of time. At the end of the run the Beckman analyzer was recalibrated.

Experimental Results

The first five runs listed in table II were taken at the maximum available GN_2 pressure of 1700 psig for a holding time of 15 min. It is known from experience that within this time conditions remain reasonably stable inside the run tank. The next two runs were conducted at reduced pressures, at the same holding time, to test for possible pressure dependence of the diffusivity. The next run was conducted at a shortened holding time to test for the known time dependence of penetration by diffusion. A final run was conducted at a GN_2 pressure of 30 psig, which is too low to establish a layer of LN_2. Since diffusion is assumed to be negligible in the absence of a liquid layer, this run permitted the response time of the oxygen analyzer to be determined.

Experimental Time History of the N_2 Mole Fraction

The time history of the N_2 content of the vapor passing through the oxygen analyzer, shown in figure 6 for a typical test (Run 2), is marked by three distinct regions: I, a sharp drop from 100% to a little under 40% in the first minute; II, a small crest in the interval 1–4 min; and III, a slow decay for times exceeding 4 min. These are shown more clearly in figure 7, which gives an expanded view of the first 10 min. The transition from one region to another indicates a gradual change in the physical process governing the time history; the lines of demarcation serve only to illustrate the approximate times when one process yields to another.

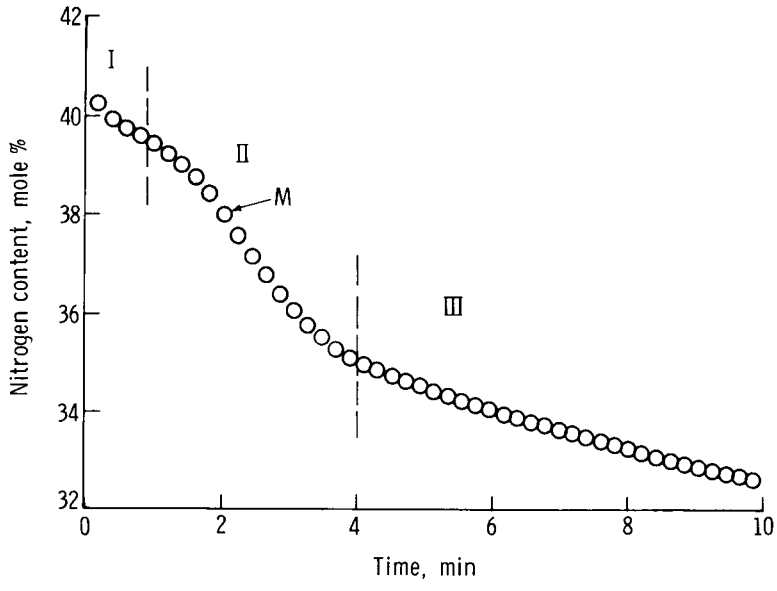

Figure 7. Expanded view of the first 10 min of figure 6. The point where the derivative has an extreme value is indicated by "*M*."

The sharp drop in region I represents the response time of the O_2 analyzer, as opposed to the transit time delay, for the transit time of the vapor from the run tank to the analyzer is estimated to be a rapid 0.2 sec at a flow rate of 30 000 cm^3/min. At the start of the analysis step (see fig. 1), the O_2 analyzer was full of pure N_2, left over from the earlier calibration. After the sample inlet valve was opened, the analyzer required a finite time to adjust to the prevailing value of the test gas. According to the instruction manual (ref. 3), the instrument requires 20 sec to reach 90% of the steady-state reading, following a step change in concentration. This figure corresponds to a time constant of 8.7 sec. In the present experiment the adjustment interval was chosen to be 5 datum sample times, or 60 sec, for this is the time it takes for the analyzer reading to reach $[1 - \exp(-60/8.7)] = 99.9\%$ of its steady-state value. The third significant figure is within the resolution of the analyzer.

The above interpretation of region I was tested in a specially designed experiment (Run 9), in which the GN_2 pressure was made too low (30 psig) to permit the buildup of a liquid layer at the interface. Consequently there was negligible penetration of N_2 into the LOX and, after blowdown, the evaporating liquid consisted of pure O_2. The resulting time history is shown in figure 8. Here a very rapid but finite decay of the N_2 mole fraction is evident. At the fifth datum point the N_2 mole fraction measures 0.7% (99.3% O_2), in good agreement with the value computed above. Thus this test confirms the existence of an adjustment interval and, as a result, the first five data points have been excluded from the evaluation of the remaining experimental runs.

The small crest appearing in region II is attributed to the evaporation of the N_2-rich portion of the liquid. In the example of figures 6 and 7 this occurs in the interval 1–4 min, when the mole fraction of N_2 drops from about 40 to 35%. At the end of this region nearly all N_2 is out of the liquid.

During the slow decay shown in region III, residual GN_2 is being flushed out of the ullage volume. Continuous mixing of the residual GN_2 with vapor from the evaporating liquid, according to assumption (6), ensures that the GN_2 content never really goes to zero.

A comparison of the experimental time history in regions II and III with the theory (eq. (12)) is beset with two major difficulties. First, the appearance of three adjustable parameters—z_0/h, τ_1, and τ_2—in the nonlinear function given in equation (12) makes a least-squares fit to the data not only computationally intractable but of questionable reliability, for the estimate of one parameter is sensitive to small errors in the estimates of the other two. Second, the parameter τ_1, which is proportional to the number of moles in the ullage volume, is thus a function of temperature, pressure, and volume. The fact that these parameters are not constant over the full duration of the decay causes assumptions (5) and (7) to be violated.

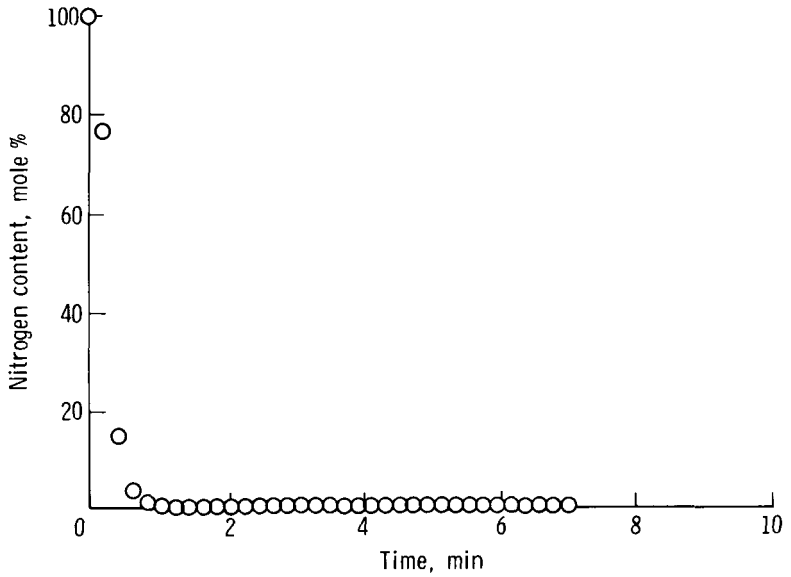

Figure 8. Time history of N_2 content in the vapor monitored by the Beckman O_2 analyzer for a low pressurization run (Run 9). The GN_2 pressure was $P = 30$ psig, too low for condensation to the liquid state, for a holding time of $t_h = 15$ min.

A simplified method of evaluating the adjustable parameters has been devised to avoid these difficulties. First, the parameter z_0/h is determined from the initial condition, equation (11), where time $t = 0$ is defined as the time of the fifth datum point. In other words, the theory is forced to fit this point.

Second, the parameter τ_1 is eliminated by the following technique. Differentiation of equation (10) yields

$$\frac{d^2x_N}{dt^2} + \frac{1}{\tau_1}\frac{dx_N}{dt} = -\frac{1}{\sqrt{\pi}\tau_1\tau_2}e^{-(t/\tau_2+z_0/h)^2} \tag{13}$$

Now, at the inflection point M (see fig. 7), $t = t_M$,

$$\left(\frac{d^2x_N}{dt^2}\right)_M = 0$$

and dx_N/dt assumes an extreme value $(dx_N/dt)_M$. Equation (13) becomes independent of τ_1:

$$\left(\frac{dx_N}{dt}\right)_M = -\frac{1}{\sqrt{\pi}\tau_2}e^{-(t_M/\tau_2+z_0/h)^2} \tag{14}$$

Since $(dx_N/dt)_M$ and t_M are known from the data, equation (14) yields τ_2. The values of τ_2 derived from equation (14) are listed in table III.

Table III. Summary of Results for Runs Used to Evaluate the Diffusivity

[N_2 pressure = 1700 psig, holding time = 15 min]

Run	x_{N0}	z_0/h	v_L, cm^3/mol	τ_2, min
1	0.171	0.6720	28.60	0.91
2	0.394	0.1895	29.34	0.79
3	0.260	0.4553	28.90	0.92
4	0.299	0.3915	29.00	0.74
5	0.181	0.6443	28.64	0.88
Mean ± standard deviation			28.90 ± 0.269	0.848 ± 0.0708

Finally τ_1, as defined in equation (8), is directly proportional to n_V, which is given by the ideal gas law:

$$n_V = \frac{PV}{R_g T} \tag{15}$$

In the early period of evaporation V and T are assumed to remain constant, but P builds up very slowly in the ullage volume. The measured time dependence of the pressure for each of the runs can be fitted to an equation of the form

$$P = 14.696 \left[b_1 + b_2 t - (b_1 - 1) e^{-b_3 t} \right] \tag{16}$$

In Run 2, for example, a fit to the pressure data yields $b_1 = 6.86$, $b_2 = 0.089827$, and $b_3 = 0.09$. If t is expressed in minutes, then equation (16) gives P in psia. Substitution of equations (15) and (16) into equation (8) leads to an expression for τ_1 of the form

$$\tau_1 = \tau_R \left[b_1 + b_2 t - (b_1 - 1) e^{-b_3 t} \right] \tag{17}$$

where τ_R is the value of τ_1 at time $t = 0$. Upon substituting equation (17) for τ_1, and inserting the values of z_0/h and τ_2 obtained from the above procedures, one finds that a fit of equation (12) to the data of figure 6 yields $\tau_R = 7.8$ min. The resulting theoretical expression is compared with experiment in figure 9. The fit is considered excellent up to the time $t = 20$ min, after which time the experimental values veer away from the theory. The reason for the discrepancy is believed to be a breakdown in the assumptions leading to equation (12), especially assumptions (5) and (7). Nevertheless, the excellent agreement during the initial 20-min period of the analysis step confirms the validity of the model, the assumptions, and the derived values of τ_1 and τ_2.

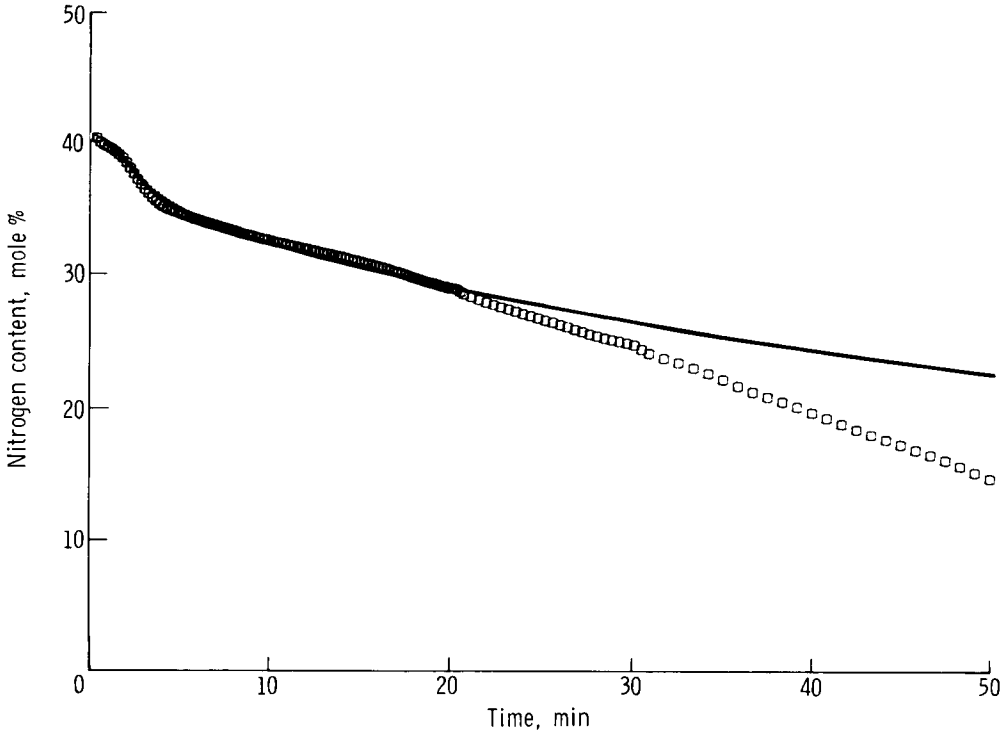

Figure 9. Best fit of equation (12) (solid line) to the time history shown in figure 6.

Evaluation of the Diffusivity

Equations (7) and (9) give the diffusivity in terms of the experimental parameters:

$$D = \frac{1}{t_h}\left(\frac{Rv_L\tau_2}{2A}\right)^2 \tag{18}$$

In order to refer the diffusivity to specific conditions, only those five runs taken at a holding pressure of 1700 psig and holding time of 15 min (Runs 1–5) were used in its final determination. The flow rate R, in mol/min, is determined from

$$R = \frac{\text{cm}^3/\text{min}}{\text{cm}^3/\text{mol}} = \frac{R_o(T_1P_o/T_oP_1)^{1/2}}{R_gT_1/P_1} = \frac{R_o}{R_g}\left(\frac{P_oP_1}{T_oT_1}\right)^{1/2} \tag{19}$$

where R_o, P_o, and T_o are the reference flow rate, pressure, and temperature of the flowmeter during calibration, P_1 and T_1 the actual pressure and temperature during the test, and R_g the universal gas constant. Substituting numerical values in equation (19) yields

$$R = \frac{29\,910\ \text{cm}^3/\text{min}}{82.053\ \text{cm}^3\text{-atm/mol-K}}\left(\frac{1 \times 1\ \text{atm}^2}{295.45 \times 297.15\ \text{K}^2}\right)^{1/2} = 1.230\ \text{mol/min} \tag{20}$$

The surface area of the liquid in the run tank is

$$A = 38.3 \times \sqrt{2} = 54.2\ \text{cm}^2 \tag{21}$$

where the factor $\sqrt{2}$ is needed because the run tanks are slanted at 45°, and the holding time is

$$t_h = 15 \times 60 = 900\ \text{sec} \tag{22}$$

The molar volume of the liquid mixture depends on that of each constituent weighted by molar content (assuming an ideal solution):

$$v_L = x_{NL}v_{LN} + (1 - x_{NL})v_{LX} = x_{NL}(v_{LN} - v_{LX}) + v_{LX} \tag{23}$$

At the start of region II, $x_{NL} = x_{N0}$ and at the end of region II, $x_{NL} \approx 0$. The value of v_L to be used in equation (18) is taken to be the mean of these two values:

$$\begin{aligned} v_L &= \frac{1}{2}\left[x_{N0}(v_{LN} - v_{LX}) + v_{LX} + v_{LX}\right] \\ &= v_{LX} + \frac{1}{2}x_{N0}(v_{LN} - v_{LX}) \end{aligned} \tag{24}$$

According to reference 4, $v_{LX} = 28.03\ \text{cm}^3/\text{mol}$ at $T = 90.2$ K. Since LN_2 is not a stable phase at this temperature at $P = 1$ atm, the value of LN_2 is assumed to be the same as that at $T = 77.3$ K, or $v_{LN} = 34.64\ \text{cm}^3/\text{mol}$ (ref. 5). Inserting these numerical values into equation (24) yields

$$v_L = 28.03 + 3.30x_{N0} \tag{25}$$

Thus v_L differs somewhat from one run to another and is listed in table III. The mean values of v_L and τ_2 over the five runs are used to evaluate the diffusivity. The numerical values given in equations (20)–(22) and table III yield for the diffusivity

$$D = 8.6 \times 10^{-5}\ \text{cm}^2/\text{sec} \tag{26}$$

Estimate of the Error

From equation (18) one can express the error in diffusivity D in terms of the errors in the experimental parameters:

$$\left|\frac{\delta D}{D}\right| = \left|\frac{\delta t_h}{t_h}\right| + 2\left|\frac{\delta R}{R}\right| + 2\left|\frac{\delta v_L}{v_L}\right| + 2\left|\frac{\delta \tau_2}{\tau_2}\right| + 2\left|\frac{\delta A}{A}\right| \tag{27}$$

where v_L and τ_2 are mean values over the five runs listed in table III.

The error in the holding time t_h has two sources. First, during pressurization, the N_2 liquifies and diffusion begins before the final pressure of 1700 psig is reached. Second, after the final pressure is reached and high-pressure valve 3410N is closed, the pressure drops back as GN_2 continues to condense. The additional time for readjustment of the pressure adds to the holding time. The uncertainty in the holding time is estimated to be ± 0.5 min. Therefore the error in t_h is estimated as

$$\left|\frac{\delta t_h}{t_h}\right| = \frac{0.5}{15} \times 100 = 3.3\% \tag{28}$$

The error in flow rate R consists of three parts, as determined from equation (19):

$$\left|\frac{\delta R}{R}\right| = \left|\frac{\delta R_o}{R_o}\right| + \frac{1}{2}\left|\frac{\delta P_1}{P_1}\right| + \frac{1}{2}\left|\frac{\delta T_1}{T_1}\right| \tag{29}$$

The error in the reference flow rate is taken from the calibration sheet as 43 cm^3/min. The errors in temperature and pressure at the flowmeter are due to fluctuations in ambient conditions, estimated to be ± 5 out of 760 torr and ± 3 out of 297 K. Then the error in R becomes

$$\left|\frac{\delta R}{R}\right| = \left(\frac{43}{30\,000} + \frac{1}{2} \times \frac{5}{760} + \frac{1}{2} \times \frac{3}{297}\right) \times 100 = 0.98\% \tag{30}$$

The error in v_L stems from errors in the handbook values of v_{LN} and v_{LX} and from the fact that x_{N0} is different for each of the runs (see eq. (24)). Since the former are considered accurate beyond the third significant figure, the error is attributed solely to variations in x_{N0} and is taken to be the standard deviation of the values of v_L listed in table III:

$$\left|\frac{\delta v_L}{v_L}\right| = \frac{0.269}{28.90} \times 100 = 0.93\% \tag{31}$$

The characteristic evaporation time τ_2 is subject to two kinds of error: systematic errors, due to uncertainties in the O_2 analyzer reading and digitization error in data acquisition; and random error, due to deviations in system behavior from that assumed in the model. The latter are believed to outweigh the former by far. The error is taken to be the standard deviation of the values of τ_2 listed in table III, which probably incorporates both kinds of error:

$$\left|\frac{\delta \tau_2}{\tau_2}\right| = \frac{0.0708}{0.848} \times 100 = 8.35\% \tag{32}$$

The surface area A of the liquid is known very precisely. The major source of error lies in the uncertainty in the 45° slant, which was determined to be $\pm 0.025°$. Thus

$$\left|\frac{\delta A}{A}\right| = (\tan 45°) \times 0.025° \times \frac{\pi}{180°} \times 100 = 0.44\% \tag{33}$$

Inserting the errors computed in equations (28)–(33) into equation (27) yields the total error in D:

$$\frac{\delta D}{D} = \pm [3.3 + 2 \times (0.98 + 0.93 + 8.35 + 0.44)]\,\% = \pm 24.7\% \tag{34}$$

Pressure and Time Dependence of the LN_2 Penetration

Table IV summarizes the experimental results for Runs 6 and 7, conducted to determine the pressure dependence of the diffusivity, and Run 8, to determine the dependence of N_2 penetration upon holding time.

Table IV. Summary of Results for Runs Used to Test the Pressure and Time Dependence of the N_2 Penetration

Run	N_2 pressure, psig	Holding time, min	x_{N0}	z_0/h	v_L, cm^3/mol	τ_2, min
6	1000	15	0.390	0.9248	29.327	0.63
7	500	15	0.0677	1.0556	28.263	0.73
8	1700	1	0.170	0.6743	28.601	0.19

From the data given in the table, the diffusivities corresponding to N_2 pressures of 1000 and 500 psig are evaluated to be $D = 4.9 \times 10^{-5}$ and 6.1×10^{-5} cm^2/sec, respectively. Although these values are lower than those measured under an N_2 pressure of 1700 psig, the difference falls within the experimental error and is not considered significant.

To investigate the time dependence, let the quantities associated with a holding time of 1 min (Run 8) be designated with a prime. Then, according to equations (7) and (9)

$$\frac{\tau_2}{\tau_2'} = \left(\frac{t_h}{t_h'}\right)^{1/2} = \left(\frac{15}{1}\right)^{1/2} = 3.87 \tag{35}$$

However, the measured ratio, according to the entries given in tables II and IV, is

$$\frac{\tau_2}{\tau_2'} = \frac{0.848}{0.19} = 4.46 \tag{36}$$

The difference between theory and experiment is 13%, well within the experimental error. This further confirms diffusion as the dominant mass transport mechanism.

Impact on 8' HTT Operations

Now that the LN_2-LOX diffusivity at 90.2 K has been established, it is possible to determine the LN_2 contamination profile in the spherical 8000-gal LOX storage vessel of the modified 8' HTT. Suppose it is specified that the LOX transferred from the storage vessel cannot have an N_2 contamination exceeding 1%. Then equation (1) can be used to predict how far below the LOX top surface the LN_2 concentration will exceed this limit for a given holding time:

$$z = 2(D\,t_h)^{1/2}\mathrm{erf}^{-1}(1 - 2x_N)$$

Using the value of diffusivity found earlier (see eq. (28)), and taking $t_h = 15$ min as a typical holding time, one finds

$$z = 2 \times (8.6 \times 10^{-5} \times 15 \times 60)^{1/2} \times \mathrm{erf}^{-1}(1 - 2 \times 0.01) = 0.9 \text{ cm}$$

Thus a layer at the top, about 1-cm thick, exceeds the contamination limit. If the top surface of the LOX happens to be at the equator of the storage vessel (worst case), the corresponding loss of LOX is 430 000 cm^3 = 113 gal. The loss is insignificant compared with the total capacity of the storage vessel.

Because the presence of any quantity of N_2, no matter how small, lowers the boiling point of LOX, the contaminated LOX in the storage vessel is superheated after blowdown and will continue to evaporate, even without heat influx, as long as the pressure remains at 1 atm. Merely maintaining the pressure at 1 atm is an effective method of purging a contaminated layer from the main body of the LOX. After an acceptable contamination level is reached, e.g., < 1 percent, then it is essential to maintain a slight overpressure in the storage vessel to inhibit further evaporation.

Comparison With Prior Measurements

Prior measurements of the LN_2-LOX diffusivity were made by two Soviet investigators, Bahrov (ref. 6) at 67.8 K and Boiko (ref. 7) at 77.8 K. Both used a version of the "gas phase" method, whereby gaseous N_2 is added to O_2 vapor, which is in equilibrium with the liquid. The diffusivity is estimated from the rate of pressure change resulting from the diffusion of N_2 into the LOX. These and the present results are summarized in table V.

Table V. Summary of Measurements of LN_2-LOX Binary Diffusion

Temperature, K	D, cm^2/sec	Method	Reference
67.8	$1.07 \times 10^{-5} \pm 5\%$	Gas phase	6
77.8	$2.8 \times 10^{-5} \pm 5\%$	Gas phase	7
90.2	$8.6 \times 10^{-5} \pm 25\%$	Differential flash vaporization	This work

The three sets of data listed in table V show a good fit to an expression of the Arrhenius form:

$$D = D_0 e^{-\frac{\Delta H}{R_g T_L}} \tag{37}$$

where T_L is the temperature of the liquid. A plot of ln D versus $1/T_L$ is a straight line, shown in figure 10 together with the experimental points. A pressure correction is appropriate for the present measurement because the two other measurements were made at low pressures. However, such a correction is difficult to estimate because, in contrast to gases and solids, no theory of diffusion in liquids has proved successful in fitting the data well. A rough estimate based on a theory of Eyring (ref. 8), in which the diffusivity varies inversely with the viscosity, increases the present value of diffusivity by about 15%. The pressure dependence of the viscosity is taken from reference 4. Nevertheless, in view of the theoretical uncertainty and the inconclusiveness of the pressure dependence indicated by the present data, a pressure correction to the diffusivity plotted in figure 10 has not been applied.

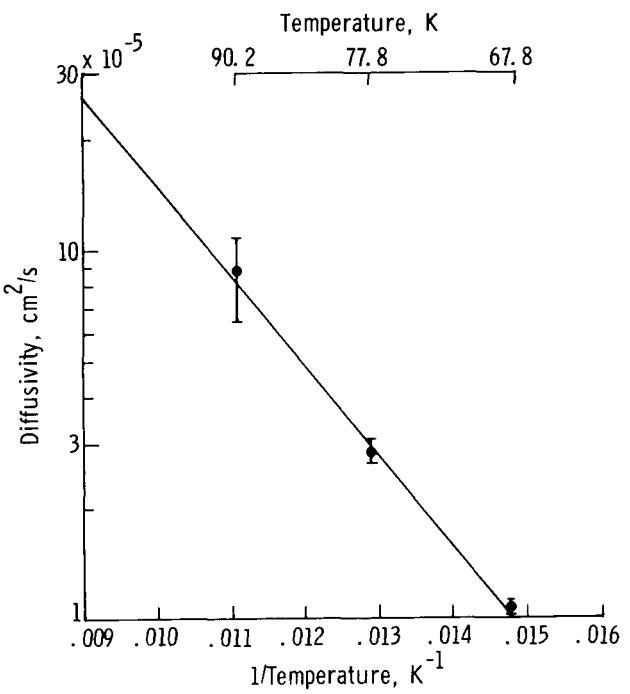

Figure 10. Arrhenius plot of the binary diffusivity: experiment (circles) and theoretical best fit (solid line).

A linear regression analysis yields the values for the preexponential factor D_0 and activation enthalpy ΔH shown in table VI. The correlation coefficient is 0.99780, indicating an excellent fit. Table VI also shows values for two other cryogenic liquid systems (refs. 9 and 10), in which the diffusivity of a dilute radioactive tracer in LN_2 was determined.

Table VI. Arrhenius Parameters for Binary Diffusion in Selected Liquid Systems

Diffusing molecule	Solvent	D_0, cm^2/sec	ΔH, kcal/mol	Method	Reference
$^{15}N_2$	$^{14}N_2$	2.38×10^{-3}	0.67	Radioactive tracer	9
Ar	N_2	1.12×10^{-3}	0.59	Radioactive tracer	10
N_2	O_2	4.52×10^{-2}	1.08	Differential flash vaporization	This work

The Arrhenius relationship expressed in equation (37) is characteristic of a thermally activated process. The associated physical model regards the liquid as having a short-range, quasi-crystalline structure with periodic potential wells. A diffusing molecule trapped in a well makes a certain number of attempts per second to jump out. The preexponential factor D_0 is proportional to the attempt frequency, and the activation enthalpy ΔH is approximately equal to the height of the potential barrier. Inspection of the values of D_0 listed in the table reveals that the attempt frequency for the N_2-O_2 system is an order of magnitude greater than that for Ar or N_2 in LN_2, and the activation enthalpy is 1.5–2 times greater. The large difference in attempt frequency is difficult to explain theoretically and must be attributed to experimental error. The difference in activation enthalpy can be explained by a possible difference in mass transport mechanisms: Transport of a tracer molecule involves a single jump over a barrier, but the binary N_2-O_2 transport could proceed by the double rotation mechanism of reference 11 and thus involve a double jump.

Conclusions

The differential flash vaporization technique has been adapted to determine the penetration of pressurized GN_2 into LOX, from which the binary diffusivity was evaluated. The mean penetration depth of five experimental runs, each at a GN_2 pressure of 1700 psig for a holding time of 15 min, was 0.9 cm. The corresponding binary diffusivity was found to be $D = 8.6 \times 10^{-5}$ cm^2/sec ±25% at a liquid temperature of 90.2 K. Tests to determine the pressure dependence of the diffusivity were inconclusive. Another test confirmed, within experimental error, the expected square-root dependence of the penetration depth on time, thus providing additional support for diffusion as the dominant mass transport process.

The measurement of the diffusivity obtained from this experiment, together with two prior measurements at lower temperatures, revealed an excellent fit to the Arrhenius equation, yielding a preexponential factor $D_0 = 4.52 \times 10^{-2}$ cm^2/sec and an activation enthalpy $\Delta H = 1.08$ kcal/mol.

The contamination of LOX by pressurized GN_2 will have but minimal impact upon operations of the modified Langley 8-Foot High-Temperature Tunnel.

NASA Langley Research Center
Hampton, VA 23665-5225
February 14, 1989

Symbols Introduced in the Appendices

a	$= \frac{2}{\tau_2}$
ΔR	correction to the evaporation rate, mol/min
s	state variable of the Laplace transform
U	flow rate of vapor leaving the ullage volume, mol/min
$X(s)$	Laplace transform of $x_N(t)$
α	$= \frac{z_0}{h}$
α'	$= \frac{z_0}{h} - \frac{\tau_2}{2\tau_1}$
β	$= \frac{1}{\tau_1}$
ξ	$= \frac{R}{U}$

Appendix A
Derivation of the Time History of the N_2 Molar Content

Applying the Laplace transform to equation (10), one obtains

$$sX(s) - x_{N0} + \frac{1}{\tau_1}X(s) = \frac{1}{2\tau_1 s} - \frac{1}{2\tau_1}\mathcal{L}\left\{\text{erf}\left(\frac{z_0}{h} + \frac{t}{\tau_2}\right)\right\} \tag{A1}$$

where $X(s)$ is $\mathcal{L}\{x_N(t)\}$. Equation (A1) can be solved for $X(s)$:

$$X(s) = \frac{x_{N0}}{s + 1/\tau_1} + \frac{1}{2\tau_1 s(s + 1/\tau_1)} - \frac{\mathcal{L}\{\text{erf}(z_0/h + t/\tau_2)\}}{2\tau_1(s + 1/\tau_1)} \tag{A2}$$

The inverse transform of the first two terms on the right are well known, but the difficulty is to find that of the third term. One proceeds by starting with the transform pair 5.12-4 in reference 12:

$$(s - \alpha)^{-1}e^{s^2}\text{erfc}(s) = \mathcal{L}\left\{e^{\alpha(t+\alpha)}\left[\text{erf}\left(\frac{1}{2}t + \alpha\right) - \text{erf}(\alpha)\right]\right\} \tag{A3}$$

Replace s by s/a and apply the scaling law:

$$\left(\frac{s}{a} - \alpha\right)^{-1} e^{(s/a)^2}\text{erfc}\left(\frac{s}{a}\right) = \mathcal{L}\left\{ae^{\alpha(at+\alpha)}\left[\text{erf}\left(\frac{at}{2} + \alpha\right) - \text{erf}(\alpha)\right]\right\} \tag{A4}$$

Now replace s by $s + \alpha a$ and apply the translation law:

$$\frac{ae^{[(s+\alpha a)/a]^2}\text{erfc}\left(\frac{s+\alpha a}{a}\right)}{(s - \alpha a + \alpha a)} = \mathcal{L}\left\{ae^{\alpha^2}e^{-\alpha at}e^{\alpha at}\left[\text{erf}\left(\frac{at}{2} + \alpha\right) - \text{erf}(\alpha)\right]\right\} \tag{A5}$$

which can be simplified to

$$\frac{e^{-\alpha^2}e^{(s/a+\alpha)^2}\text{erfc}\left(\frac{s}{a} + \alpha\right)}{s} = \mathcal{L}\left\{\text{erf}\left(\frac{at}{2} + \alpha\right) - \text{erf}(\alpha)\right\} \tag{A6}$$

Let $\alpha = z_0/h$ and $a = 2/\tau_2$ and substitute into equation (A6):

$$\frac{e^{-(z_0/h)^2}e^{(s\tau_2/2+z_0/h)^2}\text{erfc}(s\tau_2/2 + z_0/h)}{s} + \frac{\text{erf}(z_0/h)}{s} = \mathcal{L}\left\{\text{erf}\left(\frac{t}{\tau_2} + \frac{z_0}{h}\right)\right\} \tag{A7}$$

Substitute equation (A7) into (A2) and expand the last term into partial fractions:

$$X(s) = \frac{x_{N0}}{s + 1/\tau_1} + \frac{1 - \text{erf}(z_0/h)}{2\tau_1 s(s + 1/\tau_1)} - \frac{1}{2}e^{-(z_0/h)^2}e^{(s\tau_2/2+z_0/h)^2} \times \text{erfc}\left(\frac{s\tau_2}{2} + \frac{z_0}{h}\right)\left(\frac{1}{s} - \frac{1}{s + 1/\tau_1}\right) \tag{A8}$$

To evaluate the last term replace s by $s + \beta$ and apply the translation law to equation (A6):

$$\frac{e^{\left[(s+\beta)/a+\alpha'\right]^2}\text{erfc}\left[(s + \beta)/a + \alpha'\right]}{s + \beta} = \mathcal{L}\left\{e^{-\beta t}e^{\alpha'^2}\left[\text{erf}\left(\frac{at}{2} + \alpha'\right) - \text{erf}(\alpha')\right]\right\} \tag{A9}$$

Let $\beta = \frac{1}{\tau_1}$ and $\alpha' = \frac{z_0}{h} - \frac{\tau_2}{2\tau_1}$ and substitute into equation (A9):

$$\frac{e^{(s\tau_2/2+z_0/h)^2}\text{erfc}\left(s\tau_2/2 + z_0/h\right)}{s + 1/\tau_1} = \mathcal{L}\left\{e^{-t/\tau_1}e^{(z_0/h-\tau_2/2\tau_1)^2}\left[\text{erf}\left(\frac{t}{\tau_2} + \frac{z_0}{h} - \frac{\tau_2}{2\tau_1}\right) - \text{erf}\left(\frac{z_0}{h} - \frac{\tau_2}{2\tau_1}\right)\right]\right\} \tag{A10}$$

Upon applying equations (A7) and (A10) to evaluate the last terms, one finds the time history $x_N(t)$ by taking the inverse transform of equation (A8) and substituting equation (11) for x_{N0}. The solution is

$$\dot{x}_N(t) = \frac{1}{2}\left[1 - \operatorname{erf}\left(\frac{t}{\tau_2} + \frac{z_0}{h}\right)\right] + \frac{1}{2}\exp\left[-\left(\frac{t}{\tau_1} + \frac{z_0\tau_2}{h\tau_1} - \frac{\tau_2^2}{4\tau_1^2}\right)\right] \times \left[\operatorname{erf}\left(\frac{t}{\tau_2} + \frac{z_0}{h} - \frac{\tau_2}{2\tau_1}\right) - \operatorname{erf}\left(\frac{z_0}{h} - \frac{\tau_2}{2\tau_1}\right)\right] \tag{A11}$$

Appendix B

A Method of Correcting for a Slow Pressure Buildup in the Ullage Volume

A correction to the evaporation rate due to a slow pressure buildup in the ullage volume is derived in the following. From the continuity equation

$$R = U + \frac{1}{\sqrt{2}} \frac{dn_V}{dt} \tag{B1}$$

where U is the flow rate of vapor leaving the ullage volume (1.23 mole/min), which was held constant by adjustment of valve A. The factor $\sqrt{2}$ accounts for the slant of the run tank . From equation (15), parameters V and T are assumed to remain constant, but P builds up very slowly with time in the ullage volume. Therefore, equation (B1), combined with equation (15), can be expressed in the following form:

$$R = U + \frac{1}{\sqrt{2}} \frac{d}{dt} \left(\frac{PV}{R_g T} \right) = U + \frac{V}{\sqrt{2} R_g T} \frac{dP}{dt} \tag{B2}$$

Substitute the values $V = 8000$ cm^3, $R_g = 82.1$ cm^3-atm/mol-K, and $T = 90.2$ K into equation (B2) to obtain a correction to the evaporation rate:

$$\Delta R = R - U = 0.76388 \frac{dP}{dt} \tag{B3}$$

The time derivative of P follows from equation (16):

$$\frac{dP}{dt} = b_2 + b_3(b_1 - 1)e^{-b_3 t} \tag{B4}$$

where the pressure has been converted to atmospheres. Upon substituting the values of b_1, b_2, b_3 (see table B1), and $t = t_M$ (including the offset time) into equation (B4), one can evaluate ΔR.

Table B1. Summary of Results for the Correction of τ_2 Due to Pressure Buildup

Run	b_1	b_2	b_3	t_M, min	$\left(\frac{dX_N}{dt}\right)_M$, min^{-1}	$\left(\frac{dP}{dt}\right)_M$, atm/min	$\frac{d\tau_2}{\tau_2} \times 100\%$
1	3.1411	0.01168	2.0368	0.92475	−0.03547	0.035	−0.90
2	6.86	0.089827	0.09	1.33575	−0.02120	0.516	−5.88
3	3.255	0.1397	0.440	1.33575	−0.01631	0.490	−6.55
4	3.959	0.1099	0.143	1.13025	−0.01916	0.430	−5.49
5	3.973	0.18344	0.704	0.92475	−0.03609	0.713	−17.3

Next, the modified transport equation due to pressure buildup is determined by again substituting equations (2), (7), (8), and (9) into equation (6) and changing the evaporation rate R on the left-hand side to the flow rate of vapor U:

$$\frac{dx_N}{dt} + \frac{1}{\tau_1} x_N = \frac{\xi}{2\tau_1} \left[1 - \text{erf} \left(\frac{z_0}{h} + \frac{t}{\tau_2} \right) \right] \tag{B5}$$

where $\xi = R/U$ and τ_1 is redefined as n_V/U.

Differentiation of equation (B5) leads to

$$\frac{d^2 x_N}{dt^2} + \frac{1}{\tau_1} \frac{dx_N}{dt} = -\frac{\xi}{\sqrt{\pi} \tau_1 \tau_2} e^{-(z_0/h + t/\tau_2)^2} \tag{B6}$$

At the inflection point M, $\left(\frac{d^2 x_N}{dt^2}\right)_M = 0$. Thus, equation (B6) becomes

$$\tau_2 e^{(t_M/\tau_2 + z_0/h)^2} = -\frac{\xi}{\sqrt{\pi} (dx_N/dt)_M} \tag{B7}$$

By differentiating equation (B7), one obtains the correction $d\tau_2$ in the following form:

$$d\tau_2 = -\frac{1}{\sqrt{\pi}\left(\frac{dx_N}{dt}\right)_M} \frac{e^{-(t_M/\tau_2 + z_0/h)^2} d\xi}{\left[1 - 2\frac{t_M}{\tau_2}\left(\frac{t_M}{\tau_2} + \frac{z_0}{h}\right)\right]} \tag{B8}$$

where $d\xi = \Delta R/U$. The value of $d\tau_2$ is found by substituting the parameter values obtained from tables III and B1 into equation (B8). The percentage corrections to τ_2 due to pressure buildup for the 1700 psig/15 min runs are listed in the final column of table B1. The relative correction to τ_2, however, is still smaller than the error of τ_2 (except for Run 5); thus it is incorporated in the systematic and random errors of τ_2. Hence, the pressure buildup in the ullage volume did not considerably affect the experiment.

References

1. Hines, Anthony L.; and Maddox, Robert N.: *Mass Transfer—Fundamentals and Applications.* Prentice-Hall, Inc., c.1985.
2. Singh, Jag J.; Davis, William T.; and Mall, Gerald H.: *Development of a Nuclear Technique for Monitoring Water Levels in Pressurized Vessels.* NASA TM-85651, 1983.
3. Model 755 Oxygen Analyzer. Instructions 015-555422-B, Process Instruments and Controls Div., Beckman Industrial Corp., c.1985.
4. Roder, Hans M.; and Weber, Lloyd A., eds.: *ASRDI Oxygen Technology Survey, Volume I: Thermophysical Properties.* NASA SP-3071, 1972.
5. Jacobsen, R. T.; Stewart, R. B.; McCarty, R. D.; and Hanley, H. J. M.: *Thermophysical Properties of Nitrogen From the Fusion Line to 3500 R (1944 K) for Pressures to 150 000 psia (10 342 × 10^5 N/m^2).* NBS Tech. Note 648, U.S. Dep. of Commerce, Dec. 1973.
6. Bahrov, M. M.: Measurements of the Diffusion Coefficient of Nitrogen in Liquid Oxygen. *Ukr. Fiz. Zh.* (USSR), vol. 6, no. 4, 1961, pp. 486–489.
7. Boiko, V. V.: Diffusion of Nitrogen in Liquid Oxygen. *Ukr. Fiz. Zh.* (USSR), vol. 8, no. 1, 1963, pp. 135–137.
8. Eyring, Henry: Viscosity, Plasticity, and Diffusion as Examples of Absolute Reaction Rates. *J. Chem. Phys.*, vol. 4, Apr. 1936, pp. 283–291.
9. Krynicki, K.; Rahkamaa, E. J.; and Powles, J. G.: The Properties of Liquid Nitrogen. I. Self-Diffusion Coefficient. *Mol. Phys.*, vol. 28, no. 3, Sept. 1974, pp. 853–855.
10. Ricci, F. P.: Diffusion in Simple Liquids. *Phys. Review*, vol. 156, no. 1, second ser., Apr. 1967, pp. 184–190.
11. Hirschfelder, Joseph; Stevenson, David; and Eyring, Henry: A Theory of Liquid Structure. *J. Chem. Phys.*, vol. 5, Nov. 1937, pp. 896–912.
12. Erdélyi, A., ed.: *Tables of Integral Transforms, Volume I.* McGraw-Hill Book Co., Inc., 1954.

NASA
National Aeronautics and Space Administration

Report Documentation Page

1. Report No.	2. Government Accession No.	3. Recipient's Catalog No.
NASA TP-2894		

4. Title and Subtitle	5. Report Date
Contamination of Liquid Oxygen by Pressurized Gaseous Nitrogen	April 1989
	6. Performing Organization Code
7. Author(s)	8. Performing Organization Report No.
Allan J. Zuckerwar, Tracy K. King, and Kim Chi Ngo	L-16526
9. Performing Organization Name and Address	10. Work Unit No.
NASA Langley Research Center Hampton, VA 23665-5225	505-43-31-05
	11. Contract or Grant No.
12. Sponsoring Agency Name and Address	13. Type of Report and Period Covered
National Aeronautics and Space Administration Washington, DC 20546-0001	Technical Paper
	14. Sponsoring Agency Code

15. Supplementary Notes

Allan J. Zuckerwar: Langley Research Center, Hampton, Virginia.
Tracy K. King and Kim Chi Ngo: Old Dominion University, Norfolk, Virginia.

16. Abstract

The penetration of pressurized gaseous nitrogen (GN_2) into liquid oxygen (LOX) was investigated experimentally in the Langley 7-Inch High-Temperature Tunnel, the pilot tunnel for the Langley 8-Foot High-Temperature Tunnel (8' HTT). A preliminary test using a nuclear monitor revealed the extent of the liquid nitrogen (LN_2) buildup at the LOX interface as a function of GN_2 pressure. Then an adaptation of the differential flash vaporization technique was used to determine the binary diffusivity D of the LOX-LN_2 system at a temperature of 90.2 K. The measured value $D = 8.6 \times 10^{-5}$ cm^2/sec ±25% together with two prior measurements at lower temperatures revealed an excellent fit to the Arrhenius equation, yielding a preexponential factor $D_0 = 4.52 \times 10^{-2}$ cm^2/sec and an activation enthalpy $\Delta H = 1.08$ kcal/mol. At a pressure of 1700 psig and holding time of 15 min, the penetration of LN_2 into LOX (to a 1% contamination level) was found to be 0.9 cm, indicating but minimal impact upon 8' HTT operations.

17. Key Words (Suggested by Authors(s))	18. Distribution Statement
LOX contamination Diffusion Diffusivity	Unclassified—Unlimited Subject Category 34

19. Security Classif. (of this report)	20. Security Classif. (of this page)	21. No. of Pages	22. Price
Unclassified	Unclassified	24	A03

NASA-Langley, 1989
For sale by the National Technical Information Service, Springfield, Virginia 22161-2171